Journal of Applied Toxicology

WILEY

Journal of AppliedToxicology

RESEARCH ARTICLE

Exposure to Polyethylene Terephthalate Microplastic Induces Mouse Liver Fibrosis Through Oxidative Stress and p38 MAPK/p65 NF-κB Signaling Pathway

Rihao Ji[1] | Yanfang Yang[1] | Bohao Bian[2] | Yafeng Zhang[1] | Feifei Wang[3] | Yuqiao Jia[1]

[1]School of Public Health, Baotou Medical College, Baotou, Inner Mongolia, China | [2]Hulunbuir Center for Disease Control and Prevention, Hulunbuir, China | [3]State Key Laboratory of Environmental Criteria and Risk Assessment, Chinese Research Academy of Environmental Sciences, Beijing, China

Correspondence: Feifei Wang (wangfeifei826@126.com) | Yuqiao Jia (jiayuq1713@126.com)

Received: 6 December 2024 | **Revised:** 28 March 2025 | **Accepted:** 28 March 2025

Funding: This work was supported by the National Natural Science Foundation of China (42377430), the Inner Mongolia Autonomous Region Health Science and Technology Plan project (202201382), and the Bud Plan of Baotou Medical College (HLJH202418).

Keywords: liver fibrosis | microplastics | oxidative stress | p38 signaling pathway | polyethylene terephthalate

ABSTRACT

Microplastic (MP) pollution has garnered attention due to its potential impact on living organisms. Among these, polyethylene terephthalate microplastics (PET-MPs) are frequently detected in both environmental samples and human tissues. Despite this, the effects of PET-MPs on liver damage and fibrosis in mammals remain insufficiently understood. This study demonstrated that oral exposure to PET-MPs at doses of 1 mg/day (with a diameter of 1 μm) over 42 days resulted in inhibited weight gain and altered organ coefficients in male mice, suggesting possible liver damage. Using HE and Masson staining revealed pathological changes in the livers of exposed mice, such as hepatocyte swelling, inflammatory cell infiltration, and collagen deposition. Liver function tests confirmed elevated serum levels of alanine aminotransferase (ALT) and aspartate aminotransferase (AST). Further, the elevated levels of oxidative stress markers, along with the enhanced expression of proteins related to the p38 MAPK/p65 NF-κB signaling pathway as revealed by western blot analysis, both of which are strongly associated with liver damage and fibrosis. To further elucidate these mechanisms, experiments involving *N*-acetylcysteine (NAC) to counteract oxidative stress and SB203580 to inhibit p38 MAPK activation demonstrated that both interventions effectively mitigated liver fibrosis. Exposure to PET-MPs may trigger liver injury and fibrosis in mice. During this process, oxidative stress and the p38 MAPK/p65 NF-κB signaling pathway may play significant mediating roles.

1 | Introduction

With the advancement of the global economy, the environmental impact of plastic pollution has become increasingly severe. Large plastic fragments, under the influence of factors such as ultraviolet radiation, environmental weathering, air oxidation, and biodegradation, can break down into smaller particles with diameters of less than 5 mm, known as microplastics (MPs) (Li et al. 2021). The issue of MP pollution extends beyond the ocean; in fact, MP contamination on land is now proliferating at a faster rate than in marine environments (Horton et al. 2017). Humans inevitably ingest MPs through various sources such as drinking water, salt, honey, beer, and other foods (Pivokonsky et al. 2018; Waring et al. 2018; Weinstein et al. 2016). Polyethylene terephthalate (PET) is among the most common polymers found in MPs, widely used in textiles, engineering plastics, and packaging. More than half of plastic bottles and synthetic fibers are made from PET (Yoshida et al. 2016). Current studies have

Rihao Ji and Yanfang Yang contributed equally to this work.

identified MPs in human feces, with the highest concentrations being polypropylene (PP) and PET (Schwabl et al. 2019). Moreover, PET was detected in four out of 34 whole blood samples (Diamantidou et al. 2022). Research has also demonstrated that oral administration of PET affects markers of liver, heart, and kidney function in mice, and adult zebrafish exposed to PET showed accumulation in their livers (Gusevac Stojanovic et al. 2024; Lee et al. 2024).

As MPs accumulate in animal organs and are detected in human tissues, researchers are increasingly focusing on their toxic effects and underlying mechanisms. The liver, a major detoxification organ, is particularly vulnerable to the impact of MPs (Tan et al. 2024). Studies have shown that ingestion of polyethylene microplastics (PE-MPs) at a dose of 100 μg/g can induce liver inflammation and metabolic disturbances in mice, potentially exacerbating liver fibrosis (Djouina et al. 2023). Similarly, inhalation of polystyrene nanoparticles (PS-NPs) has been reported to cause liver damage and fibrosis in mice (Ge et al. 2024). Oxidative stress plays a pivotal role in the development of liver injury and fibrosis, contributing to hepatocyte necrosis, apoptosis, and exacerbation of inflammatory responses (Elmorsy et al. 2024). Previous research indicated that polystyrene microplastics (PS-MPs) in drinking water can lead to reactive oxygen species (ROS) production, stimulating Kupffer and inflammatory cells to produce profibrotic mediators, thereby activating hepatic stellate cells (HSCs) and triggering fibrosis (Wu et al. 2022). Furthermore, the mitogen-activated protein kinase (MAPK) signaling pathway is considered a key mechanism in the activation of HSCs, as it is highly sensitive to redox changes and influenced by various growth factors (Chen et al. 2020). Exposure to the plasticizer dibutyl phthalate (DBP) has been shown to promote liver fibrosis in mice through activation of the p38 MAPK signaling pathway (Huo et al. 2023). Despite these findings, the precise mechanism by which PET exposure leads to liver fibrosis in mammals remains unclear.

The primary aim of this study is to elucidate the molecular mechanisms underlying PET-MPs–induced liver fibrosis in mice. First, we confirmed that PET-MPs exposure results in liver injury, followed by an in-depth investigation into the roles of oxidative stress and the p38 MAPK/p65 NF-κB pathway in this process. Moreover, in vivo experiments showed that *N*-acetylcysteine (NAC) effectively countered oxidative damage, while SB203580 inhibited p38MAPK activation, both of which significantly mitigated PET-MPs-induced liver fibrosis. These findings suggested that NAC and SB203580 have potential as therapeutic agents for preventing PET-MPs-induced liver fibrosis. Therefore, this study provided experimental and theoretical evidence that PET-MPs exposure induces liver fibrosis in mice via oxidative stress and the p38MAPK/p65 NF-κB pathway, offering insights into potential strategies to reduce PET-MPs–related hepatotoxicity.

2 | Materials and Methods

2.1 | Characterization of PET-MPs

The PET-MPs used in this study, with a diameter of 1 μm, were procured (Shanghai Yang Li Electromechanical Technology Co.). The stock solution of PET-MPs was prepared by dissolving the particles in saline and subjecting the solution to ultrasonic vibration for 30 min. The 1-μm diameter was chosen as the standard threshold to differentiate MPs from nanoplastics (NPs) (Emenike et al. 2023). Previous studies have shown that PS-MPs with a similar diameter can induce liver fibrosis in mice (Wang et al. 2023), supporting the selection of 1-μm PET-MPs for this investigation.

2.2 | Animal and Ethics Statement

Five-week-old SPF Balb/c mice (weighing 18–22 g) were obtained from the Medical Department of Peking University (Beijing, China). The mice were housed in the Animal Facility of the School of Public Health at Baotou Medical College under standardized conditions: room temperature of 22°C ± 4°C, air humidity of 40% ± 5%, and a 12-h light–dark cycle. They had unrestricted access to sterile water and rodent feed (Keao Xieli Feed Co. Ltd., Beijing, China). All animal procedures were approved by the Medical Ethics Review Committee of Baotou Medical College (Approval No. 101, 2022).

2.3 | Experimental Protocols

PET-MPs were selected for this study because PET is a common polymer found in environmental plastic particles, including those in human feces. The dose-by-factor method was used to convert the human equivalent dose to a mouse-equivalent dose based on body surface area, using the formula: Correction factor (Km) = Weight [kg]/body surface area [m^2]. The average human weight is 60 kg, with an average body surface area of 1.62 m^2, and the average mouse weight is 0.02 kg, with a body surface area of 0.007 m^2. Thus, Km (human) = 60/1.62 = 37, and Km (mouse) = 0.02/0.007 = 3 (Nair and Jacob 2016). The estimated human intake of plastic particles ranges from 0.04 to 11.7 mg/kg per day (Senathirajah et al. 2021; Zuccarello et al. 2019). Therefore, the mouse-equivalent dose was calculated as follows: Mouse equivalent dose (mg/kg) = 0.02 × [0.04 × 37/3, 11.7 × 37/3] = [0.5, 144]. Accordingly, for a mouse weighing 0.02 kg, the dose ranges from approximately 0.01 to 2.88 mg/day. This study utilized three equivalent doses: 0.01, 0.1, and 1 mg/day.

To delve deeper into the critical roles of oxidative stress and p38 signaling pathway activation in PET-MPs–induced mouse liver fibrosis, we employed the antioxidant NAC (MedChemExpress, NJ, USA) to mitigate oxidative damage and utilized SB203580 (MedChemExpress, NJ, USA) to selectively inhibit the p38 signaling pathway. Notably, NAC, as a precursor of glutathione (GSH), demonstrated efficacy in alleviating lung injury caused by APS-NPs at a dosage of 100 mg/kg/day (Wu et al. 2023). Concurrently, SB203580, leveraging its specific capability to block the p38 signaling pathway, effectively inhibited the p38 MAPK signaling pathway at a dosage of 5 mg/kg/day, resulting in significant improvement of reproductive damage in mice (Li, Bian, et al. 2024; Xie et al. 2020).

After a 1-week acclimation period, 48 male Balb/c mice were randomly divided into eight groups of six mice each: (1) control group (saline); (2) low-dose group (0.01 mg/day PET-MPs);

(3) medium-dose group (0.1 mg/day PET-MPs); (4) high-dose group (1 mg/day PET-MPs); (5) NAC treatment group (100 mg/kg/day NAC); (6) NAC intervention group (1 mg/day PET-MPs + NAC); (7) SB203580 treatment group (5 mg/kg/day SB203580); (8) SB203580 intervention group (1 mg/day PET-MPs + SB203580).

The control group received 0.25 mL of sterile saline daily via gavage. Mice in Groups (2), (3), and (4) were administered 0.25 mL of PET-MPs solution daily at the specified concentrations. Similarly, mice in Groups (6) and (8) received daily gavage of 0.25-mL PET-MPs solution at different concentrations. Mice in Group (5) and Group (6) received intraperitoneal injections of 100 mg/kg NAC daily, while mice in Group (7) and Group (8) received intraperitoneal injections of SB203580 (5 mg/kg) every 4 days. Following 42 days of exposure, the effects of PET-MPs exposure on the liver were evaluated. The grouping and treatment of experimental animals, mice, are shown in Figure S1.

2.4 | Animal Sampling

Upon completion of the animal experiments, mice were administered a 0.3% sodium pentobarbital solution intravenously at a dosage of 50 mg/kg to facilitate blood collection. Following this, cervical dislocation was employed to euthanize the mice. Initially, the mice were weighed, after which the liver was promptly excised and weighed to determine the liver coefficient, defined as the ratio of liver weight to body weight (g/g). The left lobe of the liver from three mice per group was submerged in a 4% formaldehyde solution for preservation, whereas liver tissues from an additional three mice per group were frozen at −80°C.

2.5 | Liver Histopathology and Assessment of Liver Fibrosis Severity

The pathological changes in liver tissue were identified through hematoxylin–eosin (HE), and the extent of fibrosis in the mouse liver was evaluated using Masson's trichrome. First, liver tissues were fixed with 4% paraformaldehyde, followed by xylene dewaxing and gradient ethanol hydration. Subsequently, the treated tissues were embedded in paraffin and cut into sections with a thickness of 4 μm. Then the sections were stained with HE and Masson's trichrome. After staining, the sections were dehydrated again with ethanol of different concentrations, cleared with xylene, and finally mounted with neutral resin. Three random fields of view were selected for each section and observed with an optical microscope (BX43, Olympus, Japan) and imaging system (UC90, Olympus, Japan) to evaluate the morphological changes of the liver and the deposition areas of collagen.

2.6 | Biochemical Indicators of Mouse Liver Function

The serum was obtained from mouse blood centrifuged at 4000 rpm for 10 min and at 4°C. Then, the activities of alanine aminotransferase (ALT) and aspartate aminotransferase (AST) within the mouse serum were measured using a colorimetric method, following the guidelines specified in the kit's (Solarbio Science and Technology Co. Ltd., Beijing, China) accompanying instructions.

2.7 | Oxidative Stress Level Detection

Liver tissues were retrieved from a −80°C freezer and subsequently homogenized in PBS at a ratio of 1:9 (Liver tissue: PBS). The levels of reduced GSH, malondialdehyde (MDA), and superoxide dismutase (SOD) within the liver tissue samples were then quantified using a colorimetric assay kit (Elabscience, Wuhan, China), following the guidelines provided by the manufacturer.

2.8 | Western Bolt

Liver tissue lysates were prepared using RIPA lysis buffer (Solarbio, Beijing, China). The protein concentration in the lysates was determined using a BCA assay kit (Elabscience, Wuhan, China). Equal amounts of protein samples were separated by SDS-PAGE and transferred onto PVDF membranes. The membranes were then blocked with blocking solution and incubated with primary antibodies overnight at 4°C. The following antibodies were used: TGF-β (1:1000, AF1027, Affinity), α-SMA (1:1200, GB111364, Servicebio), P38 (1:1000, AB170099, Abcam), P-P38 antibody (1:1000, BS-2210R, Bioss), β-actin (1:3000, AF7018, Affinity), p65 (1:2000, YP-mAb-01907, Upingbio), and p-p65 (1:2000, YP-mAb-01272, Upingbio). Subsequently, the membranes undergoed a 2-h incubation with the secondary antibody (1:10,000, ZB2301, ZenBio) at ambient temperature. Finally, the protein bands were made visible through a chemiluminescent reaction (Elabscience Biotechnology, Wuhan, China).

2.9 | Statistical Analysis

For this experiment, all datasets were analyzed and visualized using GraphPad Prism 8 software for the creation of statistical graphs, while SPSS 27.0 software was employed to assess data normality. Initially, one-way analysis of variance (ANOVA) was conducted to determine whether there were statistically significant differences among the means of three or more independent groups. If the ANOVA results indicated a significant overall effect ($p < 0.05$), Tukey's honestly significant difference (HSD) post hoc test was applied to perform pairwise comparisons between all groups. A p value less than 0.05 was considered statistically significant and indicated with $^{*}p < 0.05$, $^{**}p < 0.01$, and $^{***}p < 0.001$.

3 | Results

3.1 | Exposure to PET-MPs Resulted in Liver Damage in Mice

In this study, mice were treated with varying doses of PET-MPs for 42 days to assess their impact on the liver. Compared with the control group, no significant difference in body weight

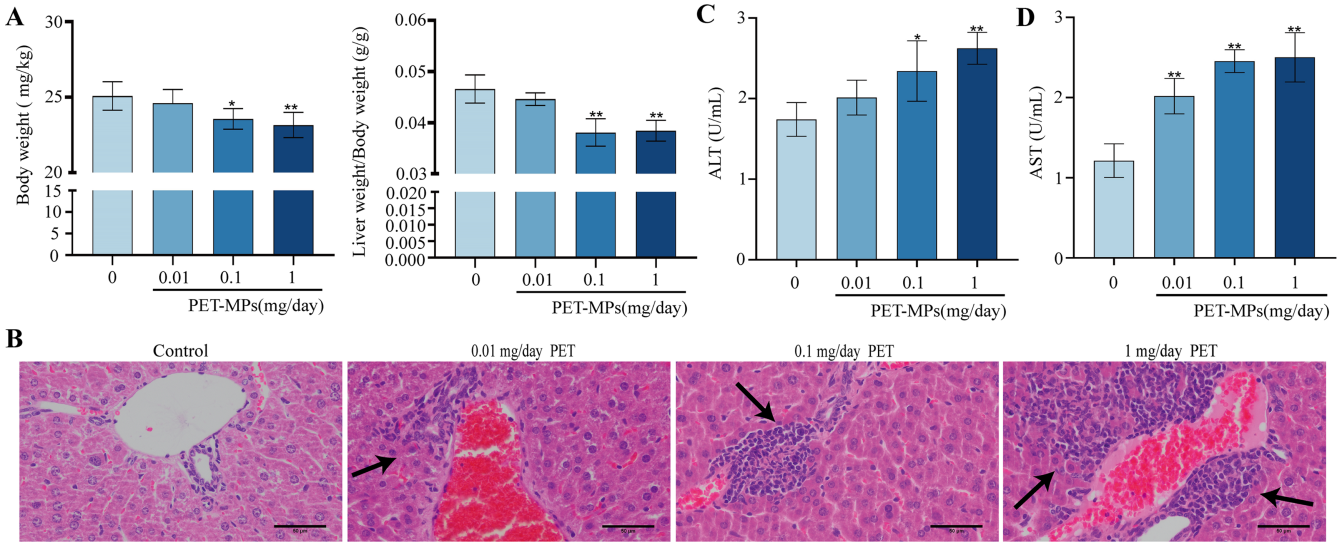

FIGURE 1 | Exposure to PET-MPs resulted in liver damage in mice. (A) Body weight and liver coefficient (liver/body weight) of mice after 42 days of poisoning. (B) HE staining of mouse liver, black arrows indicate inflammatory cell infiltration. Scale: 50 μm. (C) ALT content in mouse serum. (D) AST content in mouse serum. $n = 5$ for all groups. *$p < 0.05$, **$p < 0.01$, ***$p < 0.001$ (compared with control).

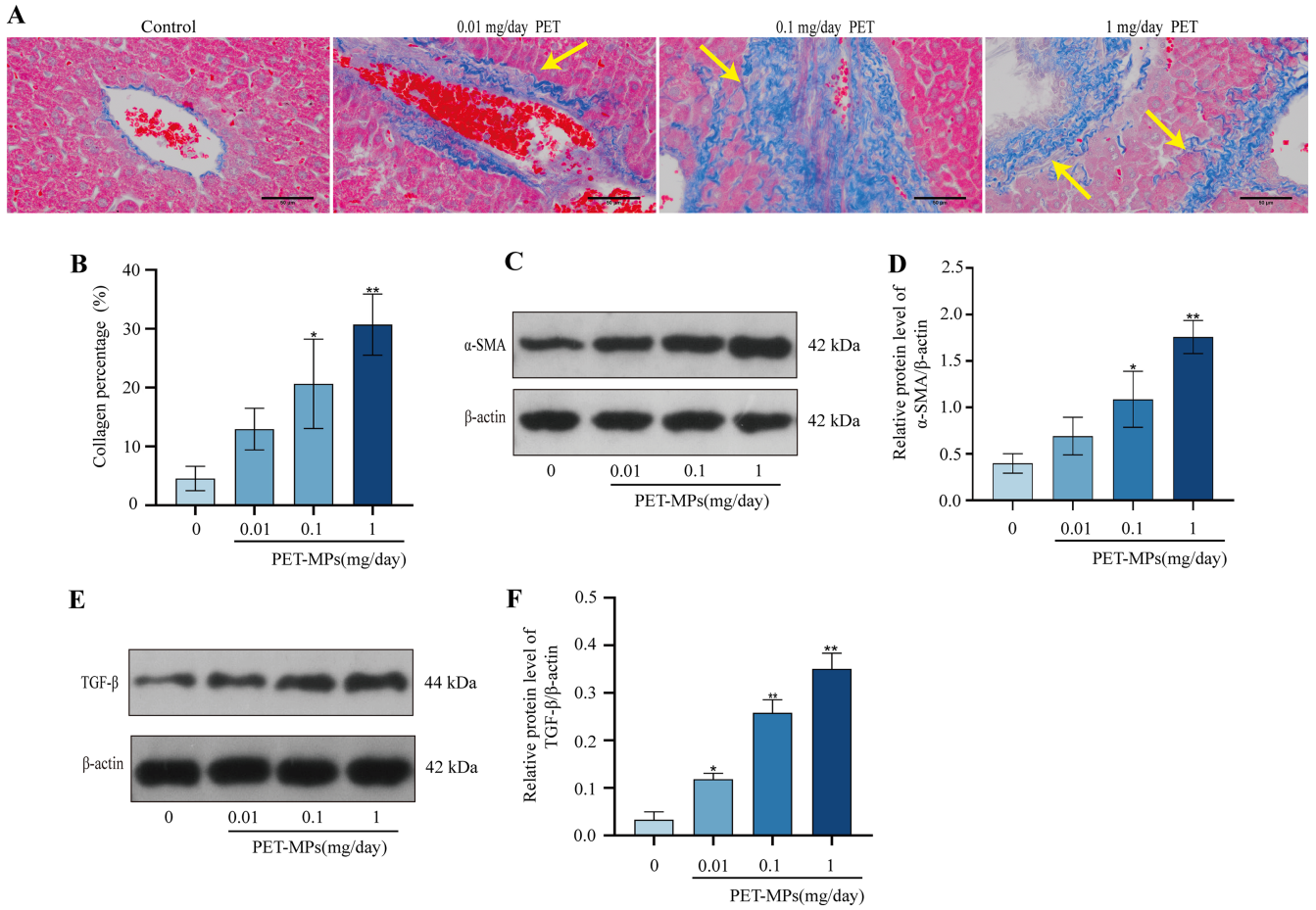

FIGURE 2 | Exposure to PET-MPs resulted in liver fibrosis in mice. (A) Masson staining of mouse liver, yellow arrows indicate collagen deposition. Scale: 50 μm. (B) Percentage of collagen fibrosis. (C) Images of α-SMA protein expression in mouse liver. (D) Quantitative analysis of α-SMA protein expression in mouse liver. (E) Images of TGF-β protein expression in mouse liver. (F) Quantitative analysis of TGF-β protein expression in mouse liver. $n = 5$ for all groups. *$p < 0.05$, **$p < 0.01$, ***$p < 0.001$ (compared with control).

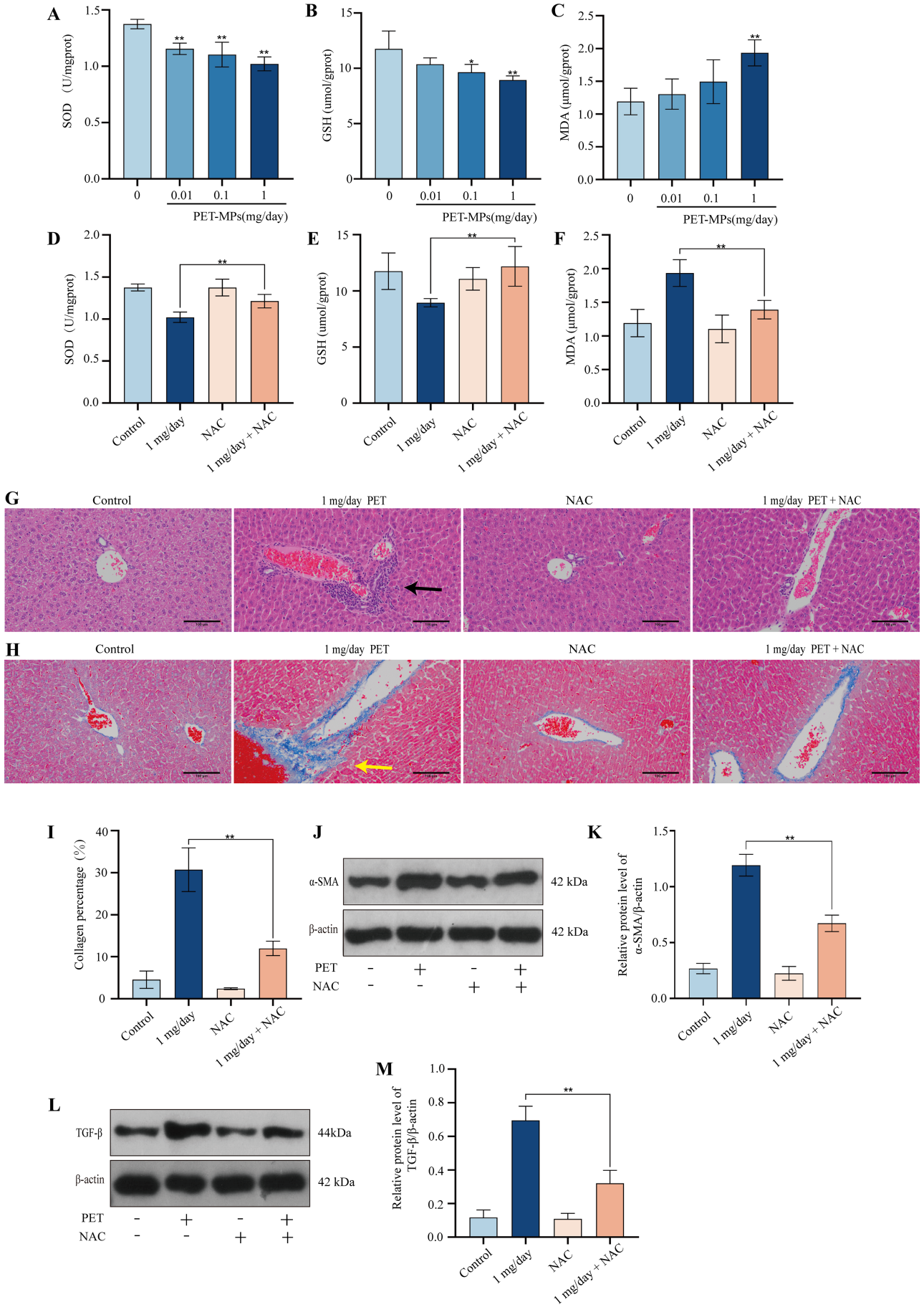

FIGURE 3 | Legend on next page.

FIGURE 3 | The role of oxidative stress in mouse liver fibrosis induced by PET-MPs. (A) SOD activity in mouse liver tissue after PET-MPs exposure. (B) GSH activity in mouse liver tissue after PET-MPs exposure. (C) MDA content in mouse liver tissue after PET-MPs exposure. (D) SOD activity in mouse liver tissue after NAC antagonism. (E) GSH activity in mouse liver tissue after NAC antagonism. (F) MDA content in mouse liver tissue after NAC antagonism. (G) HE staining of mouse liver after NAC antagonism, black arrows indicate inflammatory cell infiltration. Scale: 50 μm. (H) Masson staining of mouse liver after NAC antagonism, yellow arrows indicate collagen deposition. Scale: 50 μm. (I) Proportion of collagen fibrosis after NAC antagonism. (J) Images of α-SMA expression in mouse liver after NAC antagonism. (K) Quantitative analysis of α-SMA expression in mouse liver after NAC antagonism. (L) Images of TGF expression in mouse liver after NAC antagonism. (M) Quantitative analysis of TGF-β expression in mouse liver after NAC antagonism. $n = 5$ for all groups. $^{*}p < 0.05$, $^{**}p < 0.01$, $^{***}p < 0.001$ (compared with the corresponding intervention group).

was observed in the low-dose group ($p > 0.05$), while mice in the medium-dose and high-dose groups exhibited significantly reduced body weight in a dose-dependent manner ($p < 0.05$). Similarly, the liver coefficient (liver weight/body weight) showed no significant change in the low-dose group ($p > 0.05$), whereas a significant decrease was observed in the medium-dose and high-dose groups ($p < 0.01$) (Figure 1A). HE staining indicated that the liver cell structure of control mice was intact, with well-organized hepatic cords and no vacuoles or binucleated cells. In contrast, mice exposed to PET-MPs exhibited varying degrees of hepatic cord disarray and inflammatory cell infiltration, with damage increasing in a dose-dependent manner (Figure 1B). Liver function tests revealed a dose-dependent increase in serum ALT and AST levels in the PET-MPs exposure groups ($p < 0.05$, $p < 0.01$) (Figure 1C,D). These findings suggested that PET-MPs exposure led to both structural and functional liver damage in mice.

3.2 | Exposure to PET-MPs Resulted in Liver Fibrosis in Mice

Masson staining results revealed that, compared with the control group, there was no significant collagen fiber deposition in the low-dose group ($p > 0.05$). However, both medium-dose and high-dose groups showed significant collagen deposition (Figure 2A), with a marked increase in the proportion of collagen fibers ($p < 0.05$) (Figure 2B). Furthermore, the expression levels of α-SMA and TGF-β proteins exhibited a dose-dependent increase across the PET-MPs exposure groups ($p < 0.05$, $p < 0.01$) (Figure 2C–F). These results demonstrated that PET-MPs exposure can induce liver fibrosis in mice.

3.3 | The Role of Oxidative Stress in Mouse Liver Fibrosis Induced by PET-MPs

Following exposure to PET-MPs, levels of SOD and GSH in mouse liver tissues decreased significantly in a dose-dependent manner ($p < 0.01$), while MDA levels increased significantly ($p < 0.05$) (Figure 3A–C). These findings suggested that PET-MPs exposure induced oxidative stress in mice. To verify the role of oxidative stress in PET-MPs–induced liver injury, NAC was used as an antioxidant (Tardiolo et al. 2018). In the NAC intervention group, levels of SOD and GSH significantly increased ($p < 0.01$), while MDA levels significantly decreased ($p < 0.01$) (Figure 3D–F). Although HE staining showed no significant pathological changes in the NAC group compared with the control, the degree of liver damage was reduced compared with the PET-MPs exposure group after NAC treatment (Figure 3G). Additionally, Masson staining revealed a decrease in liver collagen deposition following NAC intervention, compared with the PET-MPs exposure group ($p < 0.01$) (Figure 3H,I). Protein expression of α-SMA and TGF-β also significantly decreased after NAC treatment compared with the PET-MPs exposure group ($p < 0.01$) (Figure 3J–M). These results indicated that oxidative stress played a critical role in PET-MPs–induced liver fibrosis in mice.

3.4 | The Role of the p38 MAPK Signaling Pathway in Mouse Liver Fibrosis Induced by PET-MPs

To investigate the effect of PET-MPs exposure on the p38 MAPK signaling pathway, we used western blot to determine the phosphorylation level of p38. The findings indicated that as the concentration of PET-MPs exposure dose, there was a significant increase in the phosphorylation level of p38 ($p < 0.01$) (Figure 4A–C). Following administration of the p38 MAPK-specific inhibitor SB203580, the phosphorylation level of p38 MAPK was markedly diminished ($p < 0.01$) (Figure 4D,E). These data indicated that PET-MPs exposure can activate the p38 MAPK signaling pathway. To further elucidate the role of the p38 MAPK signaling pathway in PET-MPs–induced mouse liver fibrosis, we performed HE observations that revealed liver tissue damage resulting from PET-MPs exposure was mitigated following SB203580 inhibition ($p < 0.01$) (Figure 4G). Similarly, compared with the PET-MPs exposure group, the proportion of liver collagen was significantly reduced after SB203580 blockade ($p < 0.01$) (Figure 4H,I). In addition, compared with the PET-MPs exposure group, the protein expression of α-SMA and TGF-β was also significantly decreased after SB203580 blockade ($p < 0.01$) (Figure 4J–M). In summary, the activation of the p38 MAPK signaling pathway played a key role in PET-MPs–induced mouse liver fibrosis.

3.5 | PET-MPs Might Initiate the Activation of the p38 MAPK/p65 NF-κB Signaling Pathway in the Liver Tissues of Mice

The MAPK pathway participates in the regulation of inflammation by modulating the downstream nuclear factor kappa B (NF-κB) pathway, while the activation of the MAPK pathway has been proven to play a crucial role in the production of inflammatory mediators and the inflammatory response (Cai et al. 2022; Zhang et al. 2024). The expression level of NF-κB p-p65 was detected using western blot. The results showed that the expression of NF-κB p-p65 significantly increased

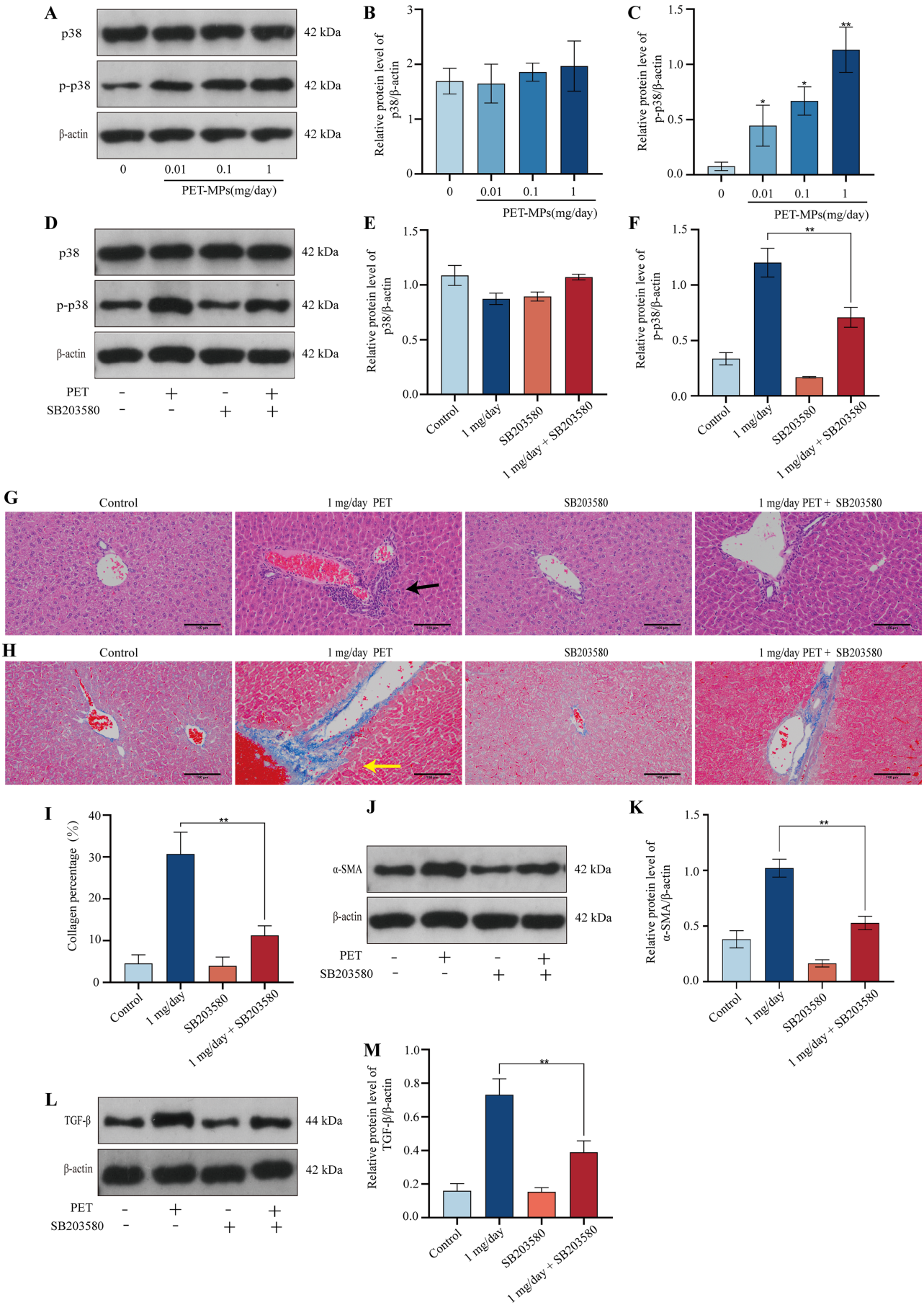

FIGURE 4 | Legend on next page.

FIGURE 4 | The role of the p38 MAPK signaling pathway in mouse liver fibrosis induced by PET-MPs. (A) Images of p38 and p-p38 expression in mouse liver tissue. (B) Quantification of p38 levels. (C) Quantification of p-p38 levels. (D) Images of p38 and p-p38 expression in mouse liver tissue after SB203580 blockade. (E) Quantification of p38 levels after SB203580 blockade. (F) Quantification of p-p38 levels after SB203580 blockade. (G) HE staining of mouse liver after SB203580 blockade, black arrows indicate inflammatory cell infiltration. Scale: 50 μm. (H) Masson staining of mouse liver after SB203580 blockade, yellow arrows indicate collagen deposition. Scale: 50 μm. (I) Proportion of collagen fibrosis after SB203580 blockade. (J) Images of α-SMA expression in mouse liver after SB203580 blockade. (K) Quantitative analysis of α-SMA expression in mouse liver after SB203580 blockade. (L) Images of TGF-β expression in mouse liver after SB203580 blockade. (M) Quantitative analysis of TGF-β expression in mouse liver after SB203580 blockade. $n = 5$ for all groups. $^{*}p < 0.05$, $^{**}p < 0.01$, $^{***}p < 0.001$ (compared with the corresponding intervention group).

with the rising concentration of PET-MPs exposure ($p < 0.01$) (Figure 5A–C); however, after treatment with SB203580, the expression of NF-κB p-p65 was significantly reduced ($p < 0.05$) (Figure 5D–F). To assess the effect of PET-MPs exposure on the inflammatory response in mice, we measured the serum levels of inflammatory markers IL-1β and IL-18 using ELISA. These results indicated that as the concentration of PET-MPs exposure increased, the levels of IL-1β and IL-18 significantly rose ($p < 0.05$) (Figure 5G,H). Furthermore, treatment with SB203580, a p38 MAPK inhibitor, significantly reduced IL-1β and IL-18 levels compared with the PET-MPs exposure group ($p < 0.01$) (Figure 5I,J). These findings indicated that PET-MPs might initiate the activation of the p38 MAPK/p65 NF-κB signaling pathway in the liver tissues of mice.

4 | Discussion

Liver fibrosis is responsible for over one million deaths annually worldwide, affecting more than one hundred million people globally (Mokdad et al. 2014; Zadorozhna et al. 2020). It is a critical stage in the progression from chronic liver disease to cirrhosis (Masuzaki et al. 2020). Previous studies have demonstrated that exposure to various types of MPs, such as PE-MPs and PS-MPs, can induce liver fibrosis in mice (Djouina et al. 2023; Shen et al. 2022). However, the mechanisms underlying PET-MPs–induced liver fibrosis remain unclear. Therefore, this study used a mouse model to investigate the effects of PET-MPs exposure on the liver, with a focus on elucidating potential molecular mechanisms.

Our findings indicated that PET-MPs exposure posed a risk of liver injury in mice. After 42 days of exposure, the mice exhibited reduced body weight and organ coefficients of liver. Histopathological analysis revealed varying degrees of inflammatory cell infiltration in the livers of PET-MPs–exposed mice, consistent with previous studies on other types of MPs, such as 1-μm PS-MPs (Shi et al. 2022). The liver enzymes ALT and AST, which are key markers of liver function, increased in a dose-dependent manner following PET-MPs exposure. These findings were consistent with Elsheikh et al.'s results, which showed that PS-MPs exposure led to increased levels of ALT and AST in mice (Elsheikh et al. 2023). Collectively, these results suggested that PET-MPs can indeed cause liver injury in mice.

HSC activation is central to liver fibrosis (Huo et al. 2023). α-SMA is recognized as a marker of HSC activation (Sui et al. 2018). Studies by Huo et al. demonstrated that dibutyl phthalate (DBP) exposure significantly increased the expression of TGF-β and α-SMA proteins, promoting liver fibrosis in mice (Huo et al. 2023). Similarly, Ge et al. found that PS-NPs exposure elevated the expression of TGF-β, α-SMA, and collagen, resulting in liver fibrosis (Ge et al. 2024). In our study, Masson's trichrome staining revealed significant collagen deposition, and PET-MPs exposure increased the relative expression levels of TGF-β and α-SMA proteins, indicating that PET-MPs can induce liver fibrosis.

The liver, a crucial metabolic organ responsible for detoxification and fat metabolism, is particularly vulnerable to oxidative stress due to its high metabolic activity and oxygen consumption. Oxidative stress occurs when ROS accumulate continuously, while antioxidants such as GSH and SOD inhibit lipid peroxidation (Fang et al. 2009). Because MDA is the final product of lipid peroxidation, its content is usually used as an indicator to measure the degree of lipid peroxidation. And the degree of lipid peroxidation is closely related to the level of ROS; therefore, the level of MDA can indirectly reflect the level of ROS (Yu et al. 2018). Our findings showed that exposure to PET-MPs resulted in decreased levels of SOD and GSH and increased MDA levels, suggesting oxidative damage in the liver. Zou et al.'s study also found decreased SOD and GSH levels and increased MDA levels in the livers of mice exposed to PS-MPs (Wang et al. 2023), supporting our results. To further investigate the role of oxidative stress in PET-MP–induced liver fibrosis, we used NAC, an antioxidant that targets ROS. NAC treatment effectively reduced inflammatory cell infiltration, collagen deposition, and the expression of TGF-β and α-SMA proteins. Additionally, NAC increased SOD and GSH levels while decreasing MDA levels. Similar findings have been reported by Li et al., who demonstrated that NAC reduced inflammatory cell infiltration and collagen deposition induced by arsenic exposure in mice, along with reducing α-SMA protein expression (Li, Li, et al. 2024). In summary, these results suggested that oxidative stress was a significant contributor to PET-MPs–induced liver fibrosis in mice (Wu et al. 2023; Yu et al. 2018).

Exposure to micro-PS induces oxidative stress, leading to the activation of the MAPK signaling pathway (Xie et al. 2020). The MAPK signaling pathway plays a crucial role in regulating cell proliferation, differentiation, and inflammatory responses (Xie et al. 2020). Our study revealed that PET-MPs exposure led to increased phosphorylation of p38 protein in the liver, which promoted the recruitment of inflammatory cells, resulting in hepatocyte infiltration and necrosis. Zhao et al. demonstrated that Di(2-ethylhexyl) phthalate (DEHP) significantly promoted hepatic fibrosis in rats by inducing oxidative stress and the production of inflammatory factors, a

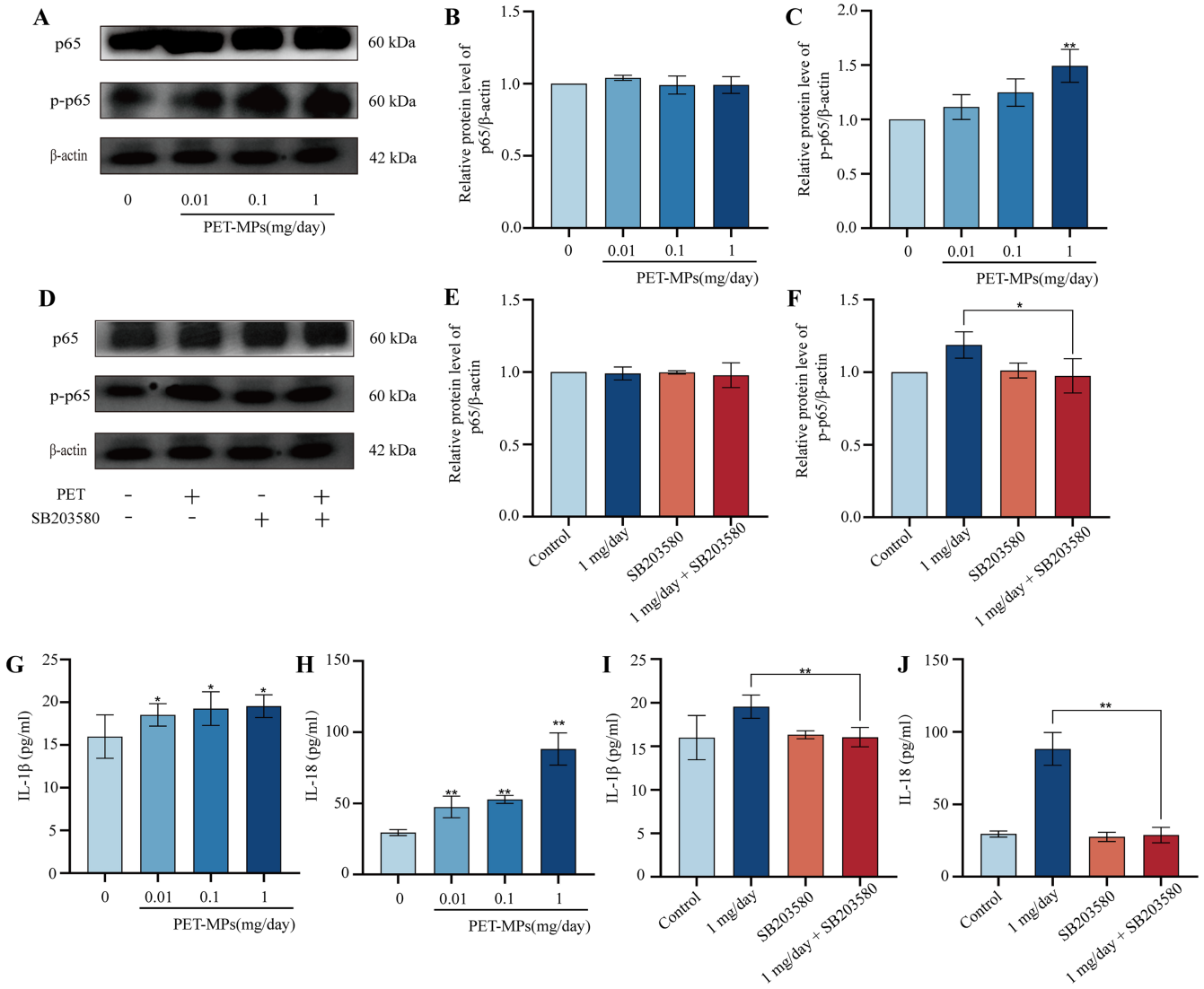

FIGURE 5 | PET-MPs might initiate the activation of the p38 MAPK/p65 NF-κB signaling pathway in the liver tissues of mice. (A) Images of p65 and p-p65 expression in mouse liver tissue. (B) Quantification of p65 levels. (C) Quantification of p-p65 levels. (D) Images of p65 and p-p65 expression in mouse liver tissue after SB203580 blockade. (E) Quantification of p65 levels after SB203580 blockade. (F) Quantification of p-p65 levels after SB203580 blockade. (G) Serum IL-1β levels in mice. (H) Serum IL-18 levels in mice. (I) Serum IL-1β levels in mice after SB203580 blockade. (J) Serum IL-18 levels in mice after SB203580 blockade. $n = 5$ for all groups. $^{*}p < 0.05$, $^{**}p < 0.01$, $^{***}p < 0.001$ (compared with the corresponding intervention group).

process associated with the activation of the p38 MAPK/NF-κB signaling pathway (Zhao et al. 2019). Similarly, Cai et al. observed that knockout of p38MAPK reduced the expression of NF-κB protein (Cai et al. 2022). Consistent with these findings, our study also revealed treatment with SB203580 significantly reduced the expression of NF-κB p-p65. The levels of inflammatory factors IL-1β and IL-18 were elevated in mouse serum, consistent with Mu et al.'s findings regarding PS-MPs exposure (Sui et al. 2018). To further elucidate the role of the p38MAPK pathway in PET-induced liver fibrosis, we used SB203580, a specific inhibitor of p38MAPK (Qiu et al. 2016). The results demonstrated that blocking p38MAPK with SB203580 significantly reduced the phosphorylation of p38, as well as the levels of IL-1β and IL-18. Additionally, SB203580 mitigated inflammatory cell infiltration and collagen deposition and decreased the expression of TGF-β and α-SMA proteins in mice. These findings were consistent with previous studies showing that SB203580 can inhibit the expression of p-p38 induced by micro-PS and reduce IL-1β levels in hepatic cell (Huo et al. 2023; Xie et al. 2020). Thus, our results suggested that PET-MPs may induce liver fibrosis by activating the p38MAPK/p65 NF-κB signaling pathway.

In summary, our study revealed that exposure to PET-MPs can lead to liver injury and fibrosis in mice. Oxidative stress and the p38MAPK/p65 NF-κB signaling pathway may play important roles in PET-MPs–induced hepatic fibrosis in mice, thus contributing essential data to inform public protection strategies and advance mechanistic research. However, this study had several limitations, including the use of only male mice, a single particle size of PET-MPs, and a limited exposure duration, which need to be further explored in future studies.

Author Contributions

Rihao Ji: writing – original draft, conceptualization, methodology, validation, data curation. **Yanfang Yang:** writing – review and editing. **Bohao Bian:** methodology. **Yafeng Zhang:** methodology. **Feifei Wang:** validation. **Yuqiao Jia:** writing – review and editing, supervision, resources, project administration, funding acquisition.

Acknowledgments

This work was supported by the National Natural Science Foundation of China (42377430), the Inner Mongolia Autonomous Region Health Science and Technology Plan project (202201382), and the Bud Plan of Baotou Medical College (HLJH202418).

Conflicts of Interest

The authors declare no conflicts of interest.

Data Availability Statement

The data that support the findings of this study are available from the corresponding author upon reasonable request.

References

Cai, M., W. Zhuang, E. Lv, et al. 2022. "Kaemperfol Alleviates Pyroptosis and Microglia-Mediated Neuroinflammation in Parkinson's Disease via Inhibiting p38MAPK/NF-κB Signaling Pathway." *Neurochemistry International* 152: 105221. https://doi.org/10.1016/j.neuint.2021.105221.

Chen, H., Q. Gan, C. Yang, et al. 2020. "Correction to: A Novel Role of Glutathione S-Transferase A3 in Inhibiting Hepatic Stellate Cell Activation and Rat Hepatic Fibrosis." *Journal of Translational Medicine* 18, no. 1: 182. https://doi.org/10.1186/s12967-020-02346-4.

Diamantidou, D., O. Mastrogianni, E. Tsochatzis, et al. 2022. "Liquid Chromatography-Mass Spectrometry Method for the Determination of Polyethylene Terephthalate and Polybutylene Terephthalate Cyclic Oligomers in Blood Samples." *Analytical and Bioanalytical Chemistry* 414, no. 4: 1503–1512. https://doi.org/10.1007/s00216-021-03741-6.

Djouina, M., C. Waxin, L. Dubuquoy, D. Launay, C. Vignal, and M. Body-Malapel. 2023. "Oral Exposure to Polyethylene Microplastics Induces Inflammatory and Metabolic Changes and Promotes Fibrosis in Mouse Liver." *Ecotoxicology and Environmental Safety* 264: 115417. https://doi.org/10.1016/j.ecoenv.2023.115417.

Elmorsy, E. A., S. Saber, R. S. Hamad, et al. 2024. "Advances in Understanding Cisplatin-Induced Toxicity: Molecular Mechanisms and Protective Strategies." *European Journal of Pharmaceutical Sciences* 203: 106939. https://doi.org/10.1016/j.ejps.2024.106939.

Elsheikh, A. A., S. M. Alnasser, A. M. Shalaby, et al. 2023. "Polystyrene Microplastic Particles Induced Hepatotoxic Injury via Pyroptosis, Oxidative Stress, and Fibrotic Changes in Adult Male Albino Rats; the Therapeutic Role of Silymarin." *Toxicology Mechanisms and Methods* 33, no. 6: 512–528. https://doi.org/10.1080/15376516.2023.2191270.

Emenike, E. C., C. J. Okorie, T. Ojeyemi, et al. 2023. "From Oceans to Dinner Plates: The Impact of Microplastics on Human Health." *Heliyon* 9, no. 10: e20440. https://doi.org/10.1016/j.heliyon.2023.e20440.

Fang, J., T. Seki, and H. Maeda. 2009. "Therapeutic Strategies by Modulating Oxygen Stress in cancer and Inflammation." *Advanced Drug Delivery Reviews* 61, no. 4: 290–302. https://doi.org/10.1016/j.addr.2009.02.005.

Ge, Y., S. Yang, T. Zhang, et al. 2024. "Ferroptosis Participated in Inhaled Polystyrene Nanoplastics-Induced Liver Injury and Fibrosis." *Science of the Total Environment* 916: 170342. https://doi.org/10.1016/j.scitotenv.2024.170342.

Gusevac Stojanovic, I., D. Drakulic, A. Todorovic, J. Martinovic, N. Filipovic, and Z. Stojanovic. 2024. "Acute Toxicity Assessment of Orally Administered Microplastic Particles in Adult Male Wistar Rats." *Toxics* 12, no. 3: 167. https://doi.org/10.3390/toxics12030167.

Horton, A. A., A. Walton, D. J. Spurgeon, E. Lahive, and C. Svendsen. 2017. "Microplastics in Freshwater and Terrestrial Environments: Evaluating the Current Understanding to Identify the Knowledge Gaps and Future Research Priorities." *Science of the Total Environment* 586: 127–141. https://doi.org/10.1016/j.scitotenv.2017.01.190.

Huo, S., B. Li, J. Du, et al. 2023. "Dibutyl Phthalate Induces Liver Fibrosis via p38MAPK/NF-κB/NLRP3-Mediated Pyroptosis." *Science of the Total Environment* 897: 165500. https://doi.org/10.1016/j.scitotenv.2023.165500.

Lee, B., E. K. Min, G. Kim, et al. 2024. "Biodistribution of Synthesized Polyethylene Terephthalate Fibers in Adult Zebrafish, Their Sex Hormone Disruption Effect, and Mitigation Using Natural Organic Matter." *Ecotoxicology and Environmental Safety* 285: 117108. https://doi.org/10.1016/j.ecoenv.2024.117108.

Li, P., X. Wang, M. Su, X. Zou, L. Duan, and H. Zhang. 2021. "Characteristics of Plastic Pollution in the Environment: A Review." *Bulletin of Environmental Contamination and Toxicology* 107, no. 4: 577–584. https://doi.org/10.1007/s00128-020-02820-1.

Li, T., B. Bian, R. Ji, et al. 2024. "Polyethylene Terephthalate Microplastic Exposure Induced Reproductive Toxicity Through Oxidative Stress and p38 Signaling Pathway Activation in Male Mice." *Toxics* 12, no. 11: 779. https://doi.org/10.3390/toxics12110779.

Li, Z., H. Li, D. Wang, X. Peng, B. M. Syed, and Q. Liu. 2024. "S-Glutathionylation in Hepatocytes Is Involved in Arsenic-Induced Liver Fibrosis Through Activation of the NLRP3 Inflammasome, an Effect Alleviated by NAC." *Science of the Total Environment* 947: 174534. https://doi.org/10.1016/j.scitotenv.2024.174534.

Masuzaki, R., T. Kanda, R. Sasaki, et al. 2020. "Noninvasive Assessment of Liver Fibrosis: Current and Future Clinical and Molecular Perspectives." *International Journal of Molecular Sciences* 21, no. 14: 4906. https://doi.org/10.3390/ijms21144906.

Mokdad, A. A., A. D. Lopez, S. Shahraz, et al. 2014. "Liver Cirrhosis Mortality in 187 Countries Between 1980 and 2010: A Systematic Analysis." *BMC Medicine* 12: 145. https://doi.org/10.1186/s12916-014-0145-y.

Nair, A. B., and S. Jacob. 2016. "A Simple Practice Guide for Dose Conversion Between Animals and Human." *Journal of Basic and Clinical Pharmacy* 7, no. 2: 27–31. https://doi.org/10.4103/0976-0105.177703.

Pivokonsky, M., L. Cermakova, K. Novotna, P. Peer, T. Cajthaml, and V. Janda. 2018. "Occurrence of Microplastics in raw and Treated Drinking Water." *Science of the Total Environment* 643: 1644–1651. https://doi.org/10.1016/j.scitotenv.2018.08.102.

Qiu, L., Y. Qian, Z. Liu, et al. 2016. "Perfluorooctane Sulfonate (PFOS) Disrupts Blood-Testis Barrier by Down-Regulating Junction Proteins via p38 MAPK/ATF2/MMP9 Signaling Pathway." *Toxicology* 373: 1–12. https://doi.org/10.1016/j.tox.2016.11.003.

Schwabl, P., S. Koppel, P. Konigshofer, et al. 2019. "Detection of Various Microplastics in Human Stool: A Prospective Case Series." *Annals of Internal Medicine* 171, no. 7: 453–457. https://doi.org/10.7326/M19-0618.

Senathirajah, K., S. Attwood, G. Bhagwat, M. Carbery, S. Wilson, and T. Palanisami. 2021. "Estimation of the Mass of Microplastics Ingested—A Pivotal First Step Towards Human Health Risk Assessment." *Journal of Hazardous Materials* 404, no. Pt B: 124004. https://doi.org/10.1016/j.jhazmat.2020.124004.

Shen, R., K. Yang, X. Cheng, et al. 2022. "Accumulation of Polystyrene Microplastics Induces Liver Fibrosis by Activating cGAS/STING Pathway." *Environmental Pollution* 300: 118986. https://doi.org/10.1016/j.envpol.2022.118986.

Shi, C., X. Han, W. Guo, et al. 2022. "Disturbed Gut-Liver Axis Indicating Oral Exposure to Polystyrene Microplastic Potentially Increases the Risk of Insulin Resistance." *Environment International* 164: 107273. https://doi.org/10.1016/j.envint.2022.107273.

Sui, M., X. Jiang, J. Chen, H. Yang, and Y. Zhu. 2018. "Magnesium Isoglycyrrhizinate Ameliorates Liver Fibrosis and Hepatic Stellate Cell Activation by Regulating Ferroptosis Signaling Pathway." *Biomedicine & Pharmacotherapy* 106: 125–133. https://doi.org/10.1016/j.biopha.2018.06.060.

Tan, S. Y., X. X. Chen, R. Zhang, et al. 2024. "SIRT3, a New Hope in Liver Diseases From Pathogenic Mechanisms to Therapeutic Strategies." *Current Pharmaceutical Biotechnology* 26. https://doi.org/10.2174/0113892010340592241011052133.

Tardiolo, G., P. Bramanti, and E. Mazzon. 2018. "Overview on the Effects of *N*-Acetylcysteine in Neurodegenerative Diseases." *Molecules* 23, no. 12: 3305. https://doi.org/10.3390/molecules23123305.

Wang, S., L. Chen, X. Shi, Y. Wang, and S. Xu. 2023. "Polystyrene Microplastics-Induced Macrophage Extracellular Traps Contributes to Liver Fibrotic Injury by Activating ROS/TGF-beta/Smad2/3 Signaling Axis." *Environmental Pollution* 324: 121388. https://doi.org/10.1016/j.envpol.2023.121388.

Waring, R. H., R. M. Harris, and S. C. Mitchell. 2018. "Plastic Contamination of the Food Chain: A Threat to Human Health?" *Maturitas* 115: 64–68. https://doi.org/10.1016/j.maturitas.2018.06.010.

Weinstein, J. E., B. K. Crocker, and A. D. Gray. 2016. "From Macroplastic to Microplastic: Degradation of High-Density Polyethylene, Polypropylene, and Polystyrene in a Salt Marsh Habitat." *Environmental Toxicology and Chemistry* 35, no. 7: 1632–1640. https://doi.org/10.1002/etc.3432.

Wu, H., T. Xu, T. Chen, J. Liu, and S. Xu. 2022. "Oxidative Stress Mediated by the TLR4/NOX2 Signalling Axis Is Involved in Polystyrene Microplastic-Induced Uterine Fibrosis in Mice." *Science of the Total Environment* 838, no. Pt 2: 155825. https://doi.org/10.1016/j.scitotenv.2022.155825.

Wu, Y., Y. Yao, H. Bai, K. Shimizu, R. Li, and C. Zhang. 2023. "Investigation of Pulmonary Toxicity Evaluation on Mice Exposed to Polystyrene Nanoplastics: The Potential Protective Role of the Antioxidant *N*-Acetylcysteine." *Science of the Total Environment* 855: 158851. https://doi.org/10.1016/j.scitotenv.2022.158851.

Xie, X., T. Deng, J. Duan, J. Xie, J. Yuan, and M. Chen. 2020. "Exposure to Polystyrene Microplastics Causes Reproductive Toxicity Through Oxidative Stress and Activation of the p38 MAPK Signaling Pathway." *Ecotoxicology and Environmental Safety* 190: 110133. https://doi.org/10.1016/j.ecoenv.2019.110133.

Yoshida, S., K. Hiraga, T. Takehana, et al. 2016. "A Bacterium That Degrades and Assimilates Poly(ethylene Terephthalate)." *Science* 351, no. 6278: 1196–1199. https://doi.org/10.1126/science.aad6359.

Yu, P., Z. Liu, D. Wu, M. Chen, W. Lv, and Y. Zhao. 2018. "Accumulation of Polystyrene Microplastics in Juvenile *Eriocheir sinensis* and Oxidative Stress Effects in the Liver." *Aquatic Toxicology* 200: 28–36. https://doi.org/10.1016/j.aquatox.2018.04.015.

Zadorozhna, M., S. Di Gioia, M. Conese, and D. Mangieri. 2020. "Neovascularization Is a Key Feature of Liver Fibrosis Progression: Anti-Angiogenesis as an Innovative way of Liver Fibrosis Treatment." *Molecular Biology Reports* 47, no. 3: 2279–2288. https://doi.org/10.1007/s11033-020-05290-0.

Zhang, Z., T. Wang, Z. Luo, et al. 2024. "Anti-Inflammatory and Analgesic Properties of Polyphyllin VI Revealed by Network Pharmacology and RNA Sequencing." *Purinergic Signal* 20, no. 4: 449–463. https://doi.org/10.1007/s11302-023-09979-2.

Zhao, Z. B., K. Ji, X. Y. Shen, et al. 2019. "Di(2-Ethylhexyl) Phthalate Promotes Hepatic Fibrosis by Regulation of Oxidative Stress and Inflammation Responses in Rats." *Environmental Toxicology and Pharmacology* 68: 109–119. https://doi.org/10.1016/j.etap.2019.03.008.

Zuccarello, P., M. Ferrante, A. Cristaldi, et al. 2019. "Exposure to Microplastics (<10 mum) Associated to Plastic Bottles Mineral Water Consumption: The First Quantitative Study." *Water Research* 157: 365–371. https://doi.org/10.1016/j.watres.2019.03.091.

Supporting Information

Additional supporting information can be found online in the Supporting Information section.